Acetyl-L-Carnitine Prevents Methamphetamine-Induced Structural Damage on Endothelial Cells via ILK-Related MMP-9 Activity

S. Fernandes[1, 2, 3]
Email silvia.fernandes@ibmc.up.pt

S. Salta [1, 2]
Email sofia.salta@ibmc.up.pt

J. Bravo [1, 4]
Email joana.bravo@ibmc.up.pt

A. P. Silva [5]
Email apsilva@cnc.cj.uc.pt

T. Summavielle [1, 2,*]
Email tsummavi@ibmc.up.pt

[1] Addiction Biology Group, IBMC - Instituto de Biologia Molecular e Celular, Universidade do Porto, Rua do Campo Alegre, 823, 4150-180 Porto, Portugal

[2] School of Allied Health Sciences, Polytechnic Institute of Porto (ESTSP-IPP), Porto, Portugal

[3] Faculdade de Medicina, Universidade do Porto (FMUP), Porto, Portugal

[4] Institute de Ciências Biomédicas de Abel Salazar (ICBAS), Universidade do Porto, Porto, Portugal

[5] Institute of Biomedical Research on Light and Image (IBILI),
Faculty of Medicine, University of Coimbra, Coimbra, Portugal

Abstract

Methamphetamine (METH) is a potent psychostimulant highly used worldwide. Recent studies evidenced the involvement of METH in the breakdown of the blood-brain-barrier (BBB) integrity leading to compromised function. The involvement of the matrix metalloproteinases (MMPs) in the degradation of the neurovascular matrix components and tight junctions (TJs) is one of the most recent findings in METH-induced toxicity. As BBB dysfunction is a pathological feature of many neurological conditions, unveiling new protective agents in this field is of major relevance. Acetyl- L-carnitine (ALC) has been described to protect the BBB function in different paradigms, but the mechanisms underlying its action remain mostly unknown. Here, the immortalized bEnd.3 cell line was used to evaluate the neuroprotective features of ALC in METH-induced damage. Cells were exposed to ranging concentrations of METH, and the protective effect of ALC 1 mM was assessed 24 h after treatment. F-actin rearrangement, TJ expression and distribution, and MMPs activity were evaluated. Integrin-linked kinase (ILK) knockdown cells were used to assess role of ALC in ILK mediated METH-triggered MMPs' activity. Our results show that METH led to disruption of the actin filaments concomitant with claudin-5 translocation to the cytoplasm. These events were mediated by MMP-9 activation in association with ILK overexpression. Pretreatment with ALC prevented METH-induced activation of MMP-9, preserving claudin-5 location and the structural arrangement of the actin filaments. The present results support the potential of ALC in preserving BBB integrity, highlighting ILK as a new target for the ALC therapeutic use.

Keywords

Blood-brain-barrier; Methamphetamine; Acetyl-L-carnitine; Tight junctions; Matrix-metalloproteinase-9; Integrin-linked kinase

Introduction

Methamphetamine (METH) is a powerful psychostimulant with high abuse liability. Both short- and long-term METH uses lead to long-lasting deleterious effects [1, 2]. METH toxicity is typically characterized by disruption of synaptic integrity and decreased monoamine production [3–5], concomitant with terminal degeneration and neuronal death [2, 6]. METH is increasingly recognized to impact also non-neuronal cells, such as microglia, and astrocytes and the blood-brain-barrier (BBB), causing the release of inflammatory

mediators and astrogliosis [1, 3, 7, 8]. The concept of METH-induced damage at the level of the BBB has gained relevance over the last few years, justifying the interest in understanding its consequences at the endothelium [4, 9, 10].

METH-induced permeability at the BBB has been consistently reported both in vivo and in vitro [4, 5, 11]. In mice models, METH was seen to increase permeability and induce massive leakage of macromolecules across the BBB in the cerebral cortex, hippocampus, and other limbic regions [5, 6, 9]. In vitro, BBB increased permeability after METH exposure was accompanied by a reduction and/or redistribution of the tight junction (TJ) proteins [7, 12–14].

The BBB is part of the neurovascular unit and is responsible for maintaining a homeostatic microenvironment for the central nervous system (CNS). Although pericytes, astrocytes, and the surrounding basement membrane play a structural and regulatory role on the neurovascular unit, the endothelial cells (ECs) are the barrier-conferring properties of the BBB [13, 15–17]. Its modulation is essentially a function of the TJ proteins [13, 16, 18–20]. Claudins, essentially claudin-5, ensure the tightness of the contact between the brain capillaries ECs, which is critical in determining BBB permeability [21, 22], while occludin plays a regulatory role and enhances TJ tightness [18]. The endothelial paracellular permeability occurs due to the equilibrium between cytoskeleton contractile forces and adhesive forces produced at the endothelial cell-cell junctions and cell-matrix contacts [14], where actin filaments play an essential role. Functioning as a cross-linker between occludin and the actin cytoskeleton, the protein *ZO-1* is also central to the TJ structure [10, 13, 18, 23].

BBB impairment with TJ dysfunction is a hallmark of many pathological states such as inflammation, tumor differentiation [24], epilepsy, Parkinson's and Alzheimer's disease, multiple sclerosis, and ischemia/reperfusion [25]. Importantly, METH-induced BBB increased permeability was associated with reduction and/or redistribution of TJ proteins [10, 13]. There is also evidence that it can interfere with structure and arrangement, which also may lead to compromised TJ function [14, 26]. Although the molecular mechanisms underlying BBB disruption under METH exposure are not fully characterized, the activation of matrix metalloproteinases (MMPs), commonly involved in remodeling and degradation of the neurovascular matrix components and therefore associated with BBB leakiness, has been reported [4, 6, 9, 27].

Investigating the mechanisms that underlie the action of compounds able to counteract these detrimental effects at the level of BBB is of major relevance. Acetyl-L-carnitine (ALC) has been described to protect the BBB function from EtOH-induced inhibition of glucose transport [28] and increased reactive oxygen species (ROS) levels [29]. ALC is a natural occurring compound synthesized from acetyl-CoA and carnitine [30–32], able to cross the BBB, essentially through organic cation transport (OCTN2) [33–35], and reaching high concentrations in the brain [30, 34]. When therapeutically administered, ALC is more easily transported across the BBB than L-carnitine, which supports its prescription in acute and

chronic neurological disorders [34]. ALC described effects include the modulation of neurotrophic factors and multiple neurotransmitters, as well as mitochondrial stabilization [30, 31], but the mechanisms involved in its action at the BBB level remain elusive.

Here, we used a model of endothelial cells exposed to ranging doses of METH to evaluate the potential protective role of ALC. Based on former reports [28, 36], we hypothesized that ALC could be protective at the BBB level by counteracting the effect of METH in the structural disruption of TJ and consequential loss of adhesive forces. We further hypothesized that ALC could be protective by preventing METH-triggered activation of MMPs.

Material and Methods

In Vitro Model and Cell Culture

The immortalized bEnd.3 cells are derived from mouse brains and known to mimic some of the BBB characteristics [37, 38]. The cell line bEnd.3 was obtained from ATCC (American Type Cell Culture-CRL-2299, Manassas, VA), and cultures were maintained in Dulbecco's Modified Eagle's medium (DMEM) (1×)/Glutamax (GIBCO®, Life Technologies, Paisley, UK), containing 5 % penicillin and streptomycin (GIBCO®, Life Technologies) and 10 % fetal bovine serum (GIBCO®, Life Technologies). Purity of the cell line was checked using an anti-CD31 antibody (Abcam 7388, rat monoclonal, 1:1000), which showed 100 % enrichment of cells on the adhesion marker. For viability assays, cells were cultured in 24-well plates (80,000 cells/well). For immunofluorescence, cells were plated on 24-well plates (80,000 cells/well) containing glass cover slips. To obtain protein extracts, bEnd. 3 cells were cultured in petri dishes (one million of cells). Cell culture media was changed every 3 days until cells were confluent.

Drug Regimen

ALC-hydrochloride was kindly provided by Sigma-Tau, S.p.a (Pomezia, Italy). METH hydrochloride was purchased from Sigma-Aldrich (St. Louis, MO, Cat.M-8750).

Immortalized bEnd.3 cells at confluence were treated with 0.25, 0.5, and 1 mM of METH, with or without a pretreatment with 1 mM ALC added 30 min prior to METH. The METH range of doses tested was predetermined in our laboratory in agreement with previous studies using METH in similar cell models [39]. The selected ALC dose of 1 mM is not toxic for the cells and is within the range of doses previously used in similar works [40]. For zymography studies, cells were treated with 10 nM BB-94 (Batimastat, Tocris Bioscience, and Bristol, UK), a broad spectrum MMP inhibitor [41], 15 min prior to METH exposure.

Cell Viability Assay—MTT

Cell viability was determined by 3-(4,5-dimethylthiazol-2yl)-2,5- diphenyl tetrazolium bromide (MTT) assay, which is based on the reduction of yellow tetrazolium salt to purple formazan crystals by metabolically active cells. The reduction of MTT is thought to mainly

occur in the mitochondria through the action of succinate dehydrogenase, therefore, providing a measure of mitochondrial function [42]. In these assay, METH concentrations of 0.25, 0.5, and 1 mM were used. Briefly, 24 h after treatment, the cells were added MTT (0.5 mg/mL, Sigma-Aldrich, Steinheim, Germany) and incubated at 37 °C. DMSO (Sigma-Aldrich) was then added to promote the dissolution of MTT-formazan crystals. Absorbance of the purple formazan was measured in duplicate by a microplate reader (Sunrise Tecan™, Mannedorf, Switzerland) at 540-nm wavelength.

Lactate Dehydrogenase Cytotoxic Assay

At 24 h of METH exposure, the LDH release to the extracellular medium was evaluated by a colorimetric assay using the CytoTox96 Non-Radioactive Assay kit (Promega, Madison, WI), according to the manufacturer's instructions. The percentage of LDH release was determined as the ratio between LDH activity in the extracellular medium and total LDH activity obtained after complete cell lysis with Triton X-100. All experiments were carried out in duplicate, using a microplate reader at 490 nm (Sunrise Tecan™).

Immunostaining Procedure

For immunocytochemistry, bEnd.3 cells were cultured on glass cover slips in 24 well plates until 90–100 % confluent. Cells were then treated with 0.5 and 1 mM of METH in the presence or absence of 1 mM ALC (added 30 min before), for 24 h. For F-actin filaments evaluation, cells were washed with phosphate buffered saline (PBS) and fixed with microtubule-protecting buffer (MPB) (65 mM PIPES; 25 mM HEPES; 10 mM EGTA; 3 mM $MgCl_2$) diluted in 4 % paraformaldehyde (pH 6.9), for 10 min. After permeabilization with Triton X-100 0.1 % for 10 min, cells were blocked with 10 % normal goat serum (NGS) for 45 min and incubated at room temperature for 1 h with Alexa488®-conjugated primary antibody (Phalloidin, Life Technologies, A12379, 1:1000). For claudin-5 and occludin, cells were washed with PBS, fixed during 15 min in methanol and permeabilized in 0.1 % Triton X-100 during 10 min. After a blocking of 45 min in 5 % BSA (bovine serum albumin), cells were incubated overnight at 4 °C with respective primary antibodies—Rabbit anti-Claudin-5 (Abcam 53765, 1:200) and Rabbit anti-occludin (Invitrogen #71–1500, 5 µg/mL). For *ZO-1* immunoreaction, a preincubation with a *preextraction* buffer (as described by Balda MS, 1996 [16]) was performed before 96 % ethanol fixation (30 min, on ice). Cells were rehydrated, permeabilized for 10 min with 0.05 % Triton X-100 and blocked for 45 min with 10 % NGS before overnight at 4 °C incubation with primary antibody (Rabbit *ZO-1*, Invitrogen #44–2200, 2.5 µg/mL). For secondary antibody incubation, we used Anti-Rabbit IgG Alexa-Fluor488® Conjugate (Cell Signaling, #4412, 1:1000), for 1 h at room temperature in the dark.

Coverslips were then mounted onto glass slides (Fluorescent Mounting Medium, CA, USA) containing 4′,6-diamidino-2-phenylindole (DAPI), and then fluorescence microphotographs were captured using AxioImager Z1 fluorescence microscope (Carl Zeiss, Germany).

Morphometric Analysis

F-actin Analysis

Changes observed on F-actin by immunofluorescence were analyzed by the Directionality plugin of Fiji Software version 2.0. This plugin is used to infer the preferred orientation of structures present in the input image. The final result is a histogram indicating the amount of filaments in a given direction (from −90 to 90°), peaking at the preferred orientation. Measurements were obtained using the Fiji Local Gradient Orientation tool that uses a 5 × 5 Sobel filter to derive the local gradient orientation [adapted from 43]. To compare different conditions, a minimum of four independent experiments was considered and an average of twelve images were captured blindly. For each condition, an average histogram was built using the mean of the amount of filaments in each bin/orientation. To analyze differences in the directionality of actin filaments, we used the interval of fifteen consecutive degrees containing the higher number of filaments for each condition.

Claudin-5 Analysis

Analysis of claudin-5 immunofluorescence images was made using the Fiji Software version 2.0. A total of four independent experiments were performed. From each coverslip, six images were blindly captured and analyzed. A straight line perpendicular to the cellular membrane limits was drawn for all cells within each image. This line was drawn always at a similar distance from the nucleus. An intensity plot profile of the line drawn was built to calculate the ratio between membrane and cytosol pixel intensity [adapted from 3]. The mean ratio of membrane/cytosol pixel intensity per condition was also calculated.

Protein Expression Analysis by Western Blot

Confluent bEnd.3 cells cultured in petri dishes were scrapped and lysed with TEN Buffer (50 mM Tris-HCl, 2 mM EDTA, 150 mM NaCl, 1 % NP-40, supplemented with phosphatases and proteases inhibitors) and then centrifuged at 14,000 × g for 15 min at 4 °C. Protein concentration of the cell lysate was estimated in the supernatant by the Bradford method (Bio-Rad Protein Assay, Munich, Germany). Proteins were loaded at 40 µg per lane and resolved by SDS-PAGE on 10 to 12 % Bis/acrilamide gels and then transferred onto PVDF membranes. After blocking with dry milk 5 %, membranes were incubated with rabbit polyclonal antibodies to claudin-5 (Abcam 53765, 1:500), occludin

(Invitrogen #71–1500, 2 µg/mL), *ZO-1* (Invitrogen #44–2200, 2 µg/mL), and mouse polyclonal antibody to GAPDH (glyceraldehyde-3-phosphate dehydrogenase, Hytest #5G4, 1:300000). Secondary antibody horseradish peroxidase (HRP)-conjugated were used for 1-h incubation. Chemiluminescence signal detection was performed using the traditional developer, using Immun-Star HRP (Bio-Rad Laboratories, USA). A GS800 densitometer (Bio-Rad) and Quantity One 1-D analysis software (v4.6, Bio-Rad) were used for densitometry analysis.

Subcellular Fractionation

Confluent monolayers were scrapped and lysed on fractionation buffer (250 mM sucrose, 20 mM HEPES (pH 7.4), 10 mM KCl, 1.5 mM $MgCl_2$, 1 mM EDTA and 1 mM EGTA) supplemented with 1 mM DTT and protease inhibitor cocktail, for 20 min. Lysates were aspirated at least 10 times through a 25 G needle in a 1-mL syringe and left on ice for 20 min. A 5-min centrifugation at 720 G was performed to centrifuge out the nuclear pellet, and the supernatant was re-centrifuged for 5 min at 10,000 G. The membrane and the cytoplasmic fractions were separated by ultracentrifugation at 100.000 G for 1 h (ultracentrifuge Beckman Coulter, 70.1 Ti Rotor, CA, USA). The supernatant (cytoplasmic fraction) was collected, and the pellet obtained was washed in fractionation buffer and resuspended with a 25 G needle as above. The membrane fraction was re-centrifuged for45 min, and the final pellet was resuspended in fractionation buffer supplemented with 10 % glycerol and 0.1 % SDS. The cytoplasmic fraction was concentrated through a filter unit (Amicon Ultra Centrifugal Filters, UFC501024). All steps were carried out at 4 °C.

Both membrane and cytoplasmic protein concentrations were determined as described above. Western blot was used to analyze tight junction amount in each fraction.

MMPs Gelatinolytic Assay

Culture-conditioned media from bEnd.3 cells was collected in confluent serum-free monolayers from each condition for determination of MMP-2 and MMP-9 activities. The collected medium was centrifuged (8000 g, 5 min) to remove cell debris and applied in a non-reducing SDS-PAGE containing 0.1 % gelatin. The electrophoresed gels were washed twice for 30 min in 2 % Triton X-100 at room temperature and incubated for 16 h at 37 °C in the substrate buffer (50 mM Tris-HCl, pH 7.5; 10 mM $CaCl_2$) to allow gelatin digesting by MMP-2 and MMP-9. After staining with 0.1 % Coomassie Brilliant Blue R-250, the gels were destained (in 20 % methanol and 10 % acetic acid) and the enzyme-digested regions were seen as clear bands against a blue background. The visualized bands were quantified by densitometry using GS800 densitometer and Quantity One 1-D Analysis software, v4.6.

Transfection and ILK Silencing

Integrin-linked kinase (ILK) knockdown was performed using small hairpin RNA (shRNA)-mediated silencing technology from SIGMA (Mission shRNA). The clone TRCN0000022517 was used in HEK293T cells to the lentivirus production. After 48 h, virus was collected and frozen. For infection, bEnd.3 cells were treated for 12 h at 37 °C with lentivirus diluted in DMEM (1×)/Glutamax (GIBCO®, Life Technologies, Paisley, UK), containing 5 % penicillin and streptomycin (GIBCO®, Life Technologies) and 10 % fetal bovine serum (GIBCO®, Life Technologies) containing 5 µg/mL polybrene. Afterwards, the virus containing medium was replaced by fresh medium. Selection of infected cells was done with puromycin treatment (2 µg/mL). ILK silencing (KD ILK) was

monitored and confirmed by Western blot using mouse anti-ILK (BD Pharmigen #611802, 1:1000). In this experiment, cells treated with control viral DNA (empty vector) are indicated as pLKO.1 and were used as a control.

Statistical Analysis

Results from at least four independent experiments were represented as mean ± SEM. Significant differences between groups were determined by one-way ANOVA followed by the Bonferroni post hoc test. When data normality was not verified, the *Kruskal-Wallis* test was used.

Significance was set at $p < 0.05$. All analysis was conducted using the software GraphPad Prism® 6.0 for Mac OSX (GraphPad Software, La Jolla CA).

Results

METH-Induced Loss of Viability in bEnd.3 Cells

The viability of bEnd.3 cultures under different doses of METH and ALC was evaluated both by MTT and LDH assays. MTT results showed that mitochondrial activity was only affected by METH 1 mM, which was significantly reduced when compared to the control condition ($p < 0.05$) (Fig. 1a). ALC 1 mM added to the cells 30 min before METH 1 mM did not prevent the decrease in the viability of bEnd.3 cells. The results provided by the LDH assay confirmed the increased toxicity of METH 1 mM, which led to significant cell loss when compared to the control ($p < 0.001$). In accordance with the data provided by the MTT assay, ALC 1 mM in combination with METH could not prevent bEnd.3 cell death (Fig. 1b).

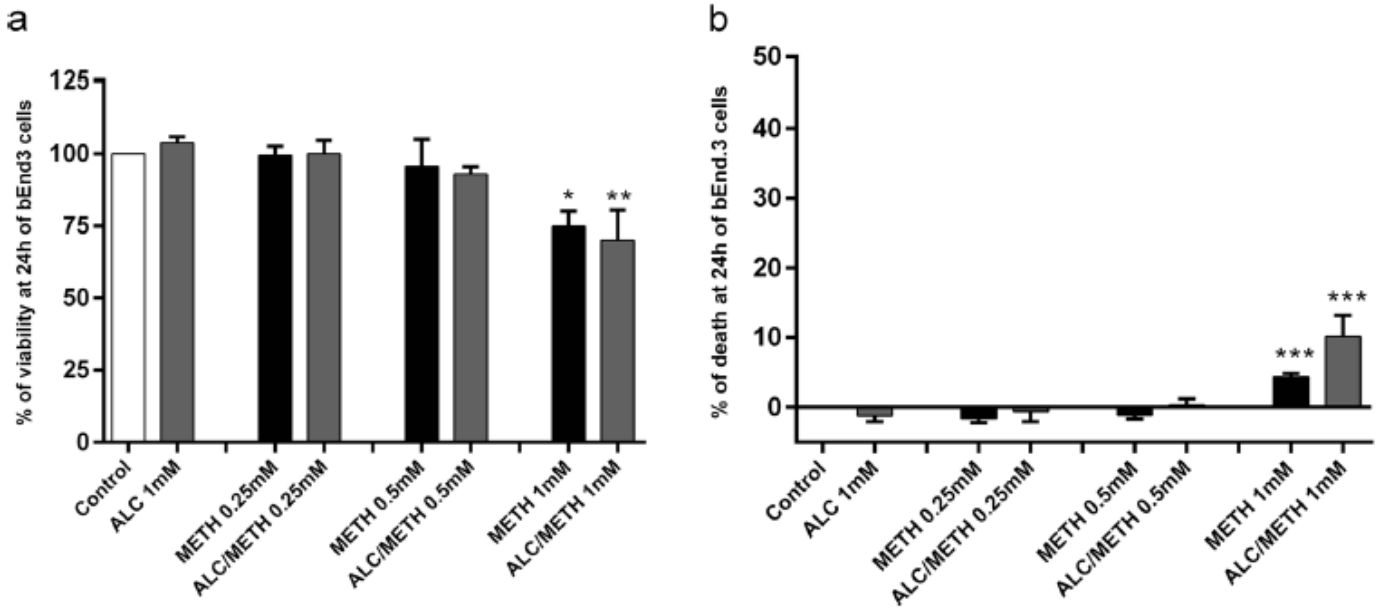

Fig 1 - Viability/cytotoxicity assays: a MTT assay, b LDH assay. Confluent bEnd.3 cells monolayers were treated with ranging concentration of METH and ALC 1 mM. a MTT reduction was assessed 24 h after treatment. b Cell death was measured by lactate dehydrogenase released on the bEnd.3 culture medium at the same time point. Data represent mean ± SEM. Significant differences are marked as *$p < 0.05$, **$p < 0.01$, and * **$p < 0.001$

compared to the control group (as determined by ANOVA followed by the Bonferroni post hoc test)

ALC Prevented the METH-Induced Loss of F-Actin Filaments Alignment

F-actin filaments organization is characteristic of adhered and immobile endothelial cells. Using phalloidin to visualize F-actin, we observed a dose-dependent loss of stress fibers organization induced by METH (Fig. 2a). This loss of organization was quantified through measuring the directionality of the filaments within the different conditions using a derivative of the original image (Fig. 2b). In the control condition, F-actin filaments are mostly organized in a single orientation, with a high proportion of filaments aligned at the same direction. The filaments organization is progressively lost when cells are exposed to increasing doses of METH, as evidenced through directionality quantification (Fig. 2c). Importantly, pretreatment with ALC 1 mM prevented the loss of organization induced by METH 1 mM as shown in Fig. 2d and e, where the majority of filaments were in a single direction (control vs METH 1 mM $p < 0.0001$; ALC/METH 1 mM vs METH 1 mM, $p < 0.05$).

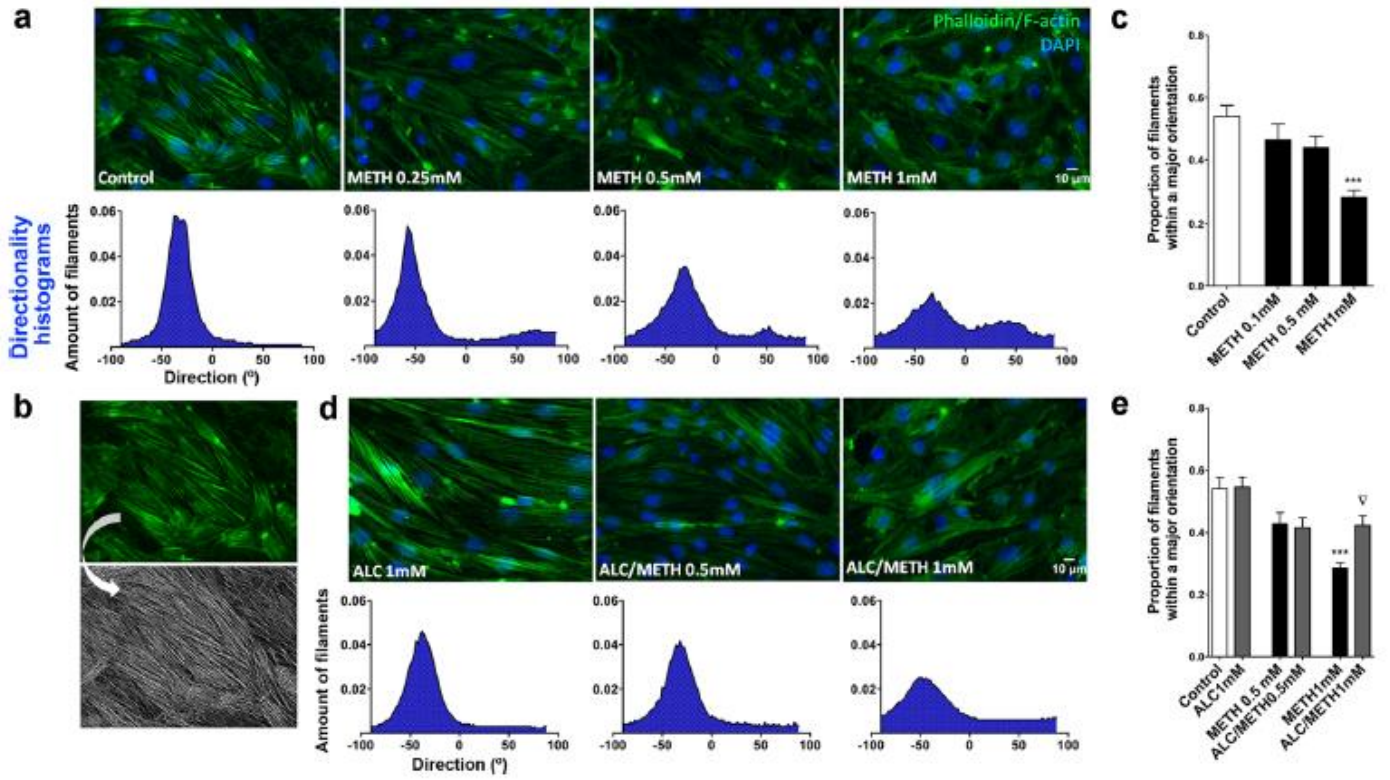

Fig 2 - F-actin filaments alignment. Confluent bEnd.3 cells monolayers were treated with METH 0.5 and 1 mM doses according to the described procedures. a Representative images are shown for F-actin filaments stained with Alexa Fluor® 488-Phalloidin and nuclei labeled with DAPI, after METH exposure. The mean histogram for each condition is represented below the respective image. **b** Changes on F-actin filaments alignment were analyzed

by the Directionality plugin of Fiji Software, using the local gradient orientation method to derive the image. **c** Proportion of actin filaments in a preferential direction after METH exposure. **d** F-actin filaments stained with Alexa Fluor® 488-Phalloidin and labeled with DAPI, when cells were pretreated with ALC 1 mM before METH exposure. The mean histogram for each condition is represented below the respective image. **e** Proportion of actin filaments in a preferential direction in cells treated with ALC 1 mM before METH exposure. Data represent mean ± SEM. ***$p < 0.001$ compared to control group; $\nabla p < 0.05$ compared to METH 1 mM (as determined by ANOVA followed by the Bonferroni post hoc test)

ALC Prevented the METH-Induced Loss and Redistribution of Claudin-5

METH-induced changes in claudin-5 were previously reported [3, 9,10]. Here, we aimed to assess the effect of ALC 1 mM in preventing these changes. Indirect immunofluorescence results showed that while in control conditions, claudin-5 is localized in the cellular membrane, after METH-exposure claudin-5 is also present in the cytoplasm (Fig. 3a and b). The ratio membrane/cytoplasm for claudin-5 localization is significantly decreased when cells are exposed for 24 h to METH ($p < 0.0001$ for both METH 0.5 and 1 mM) compared to the control (Fig. 3b). In addition, the total amount of claudin-5 was also significantly decreased after exposure to METH, as shown by Western blot analysis ($p < 0.01$ for both METH 0.5 mM and 1 mM, compared to the control, Fig. 3c). To confirm the impact of METH on claudin-5 distribution, we performed a subcellular fractionation analysis, which confirmed an increase of cytoplasmatic claudin-5 content in cells treated with METH 1 mM ($p < 0.01$, Fig. 3d).

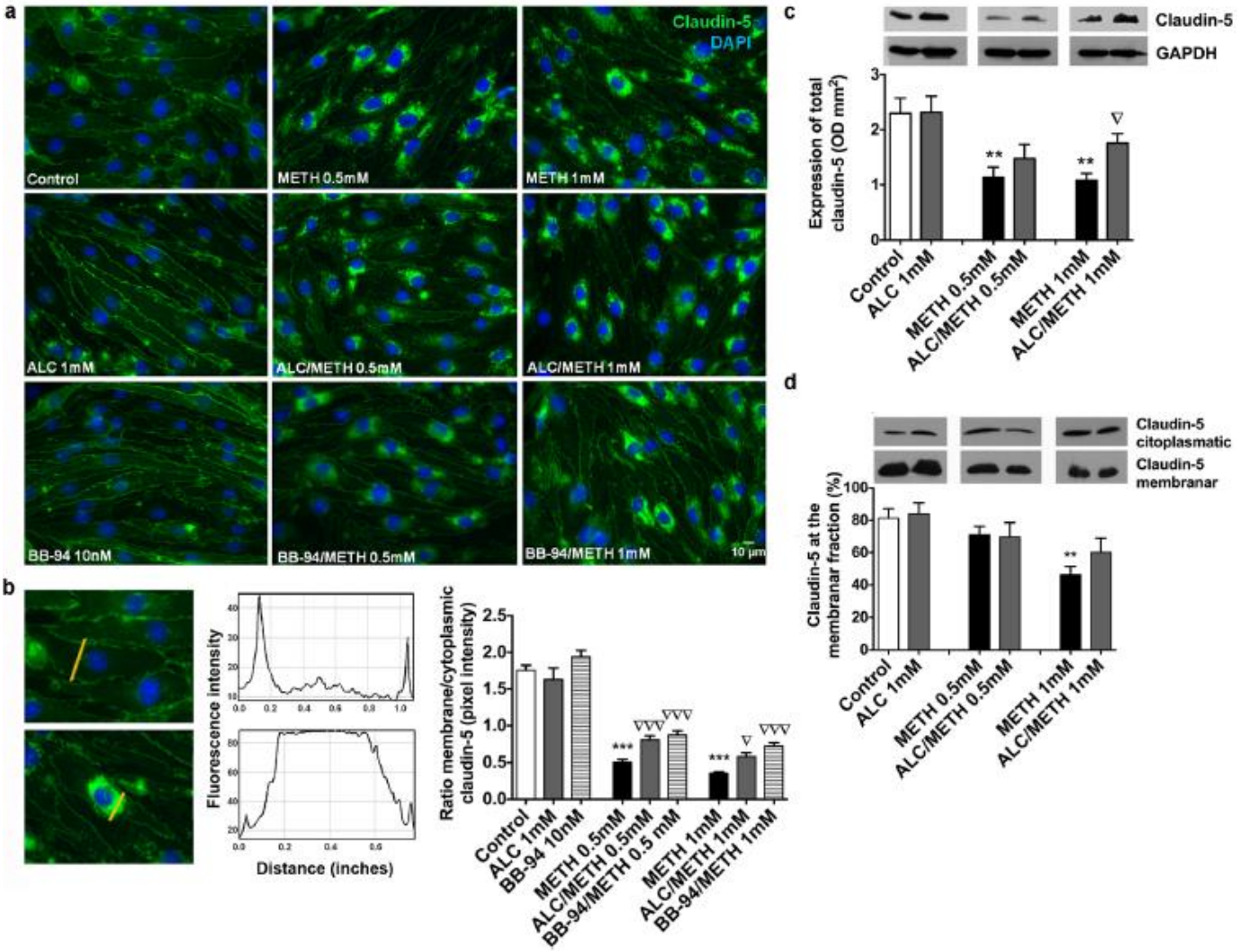

Fig 3 - Claudin-5 decrease and redistribution. Confluent bEnd.3 cells monolayers were treated with METH 0.5 and 1 mM, with or without ALC 1 mM or BB-94 10 nM. **a** Immunofluorescence representative images stained for claudin-5 and nuclei (DAPI). **b** Plot intensity profile for claudin-5 immunofluorescence obtained by drawing a straight line in each cell, always at the same position (Fiji Software), which enables to calculate the ratio between membrane and cytoplasm pixel intensity. (**c**) Total amount of claudin-5 determined by Western blot, mean ratio for each condition are represented. (**d**) Claudin 5 quantification after subcellular fractionation of the cytoplasmatic and membranar portions. Data represent mean ± SEM. Significant differences are marked as $*p < 0.05$; $**p < 0.01$, and $***p < 0.001$ compared to control; $\nabla\nabla\nabla p < 0.001$ and $\nabla p < 0.05$ compared to the respective METH dose (as determined by ANOVA followed by the Bonferroni post hoc test)

Aiming to evaluate the ability of ALC to prevent the METH-induced redistribution of claudin-5, we treated cells with ALC 1 mM. The redistribution of claudin-5 after METH exposure was partially prevented when ALC 1 mM was used, as shown by immunofluorescence images (Fig. 3a) for both doses (METH 0.5 mM vs control $p < 0.001$, METH 1 mM vs control $p < 0.05$, Fig. 3b). Total claudin-5 quantification by Western blot also evidenced a protective effect of ALC, although significance was only reached for METH 1 mM dose ($p < 0.05$, Fig. 3c). When the quantification was performed separately in both subcellular fractions, significance for the protective effect of ALC was not achieved ($p = 0.22$).

METH did not Affect Occludin and *ZO-1*

We investigated also the effect of METH exposure in *ZO-1* and occludin. In our in vitro model, METH failed to induce any significant change in occludin or *ZO*-1, both when evaluated by immunofluorescence (Fig. 4a and d) or Western blot (Fig. 4b and e). To further confirm this, we performed an evaluation by subcellular fractionation, where occludin levels on the membrane and cytoplasmic fractions were shown to be unaltered after METH or ALC treatment (Fig. 4c).

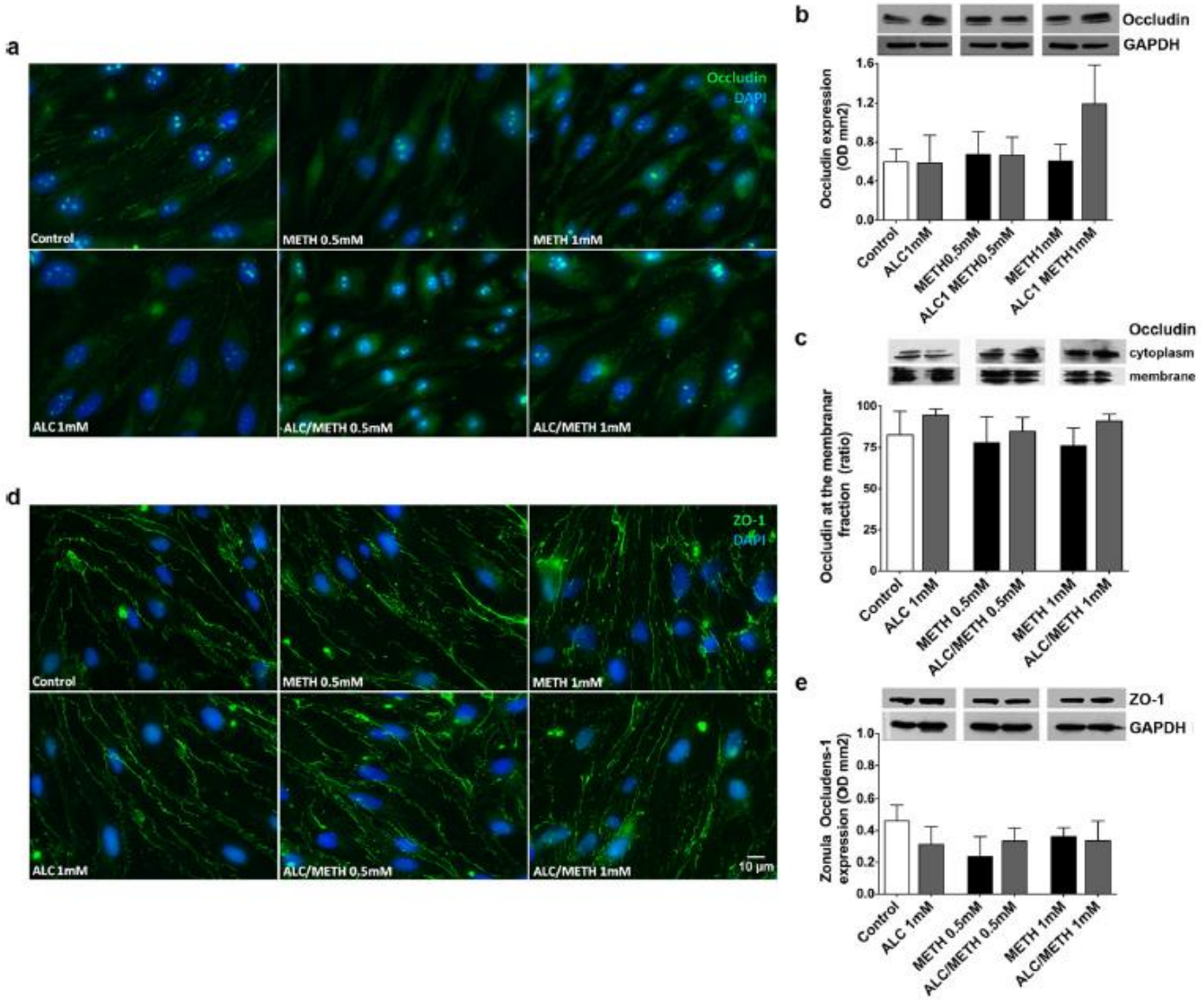

Fig 4 - METH effects on occludin and Zonnula ocludens-1. *Confluent bEnd.3 cells monolayers were treated with METH 0.5 and 1 mM, with or without the pretreatment with ALC 1 mM.* ***a*** *Immunofluorescence representative images stained for occludin nuclei (DAPI).* ***b*** *Total amount of occludin determined by Western blot.* ***c*** *Occludin quantification after subcellular fractionation of the cytoplasmatic and membranar portions;* ZO-1. ***d*** *Immunofluorescence representative images stained for* ZO-1 *and nuclei (DAPI).* ***e*** *Total amount of* ZO-1 *determined by Western blot. Data represent mean ± SEM. No significant differences were observed (as determined by ANOVA followed by the Bonferroni post hoc test)*

ALC Prevented METH-Induced MMP-9 Activity

As activation of MMPs is a common mechanism of BBB leakiness, we investigated also if

the translocation of claudin-5 mechanism could be linked to METH-triggered MMPs activation. To understand if both MMP-2 and MMP-9 gelatinases were triggered by METH, gelatinolytic assays were performed. Our results show that MMP-9 release to the medium was increased by both METH 0.5 mM and 1 mM (Fig. 5a). The increased activity was observed for METH 0.5 mM 12 h postexposure ($p < 0.05$) and 16 h postexposure for METH 1 mM ($p < 0.05$, Fig. 5a). This effect was higher at 24 h ($p < 0.001$ for METH 0.5 mM and $p < 0.01$ for METH 1 mM vs control). MMP-2 activity was not significantly affected by METH exposure (data not shown).

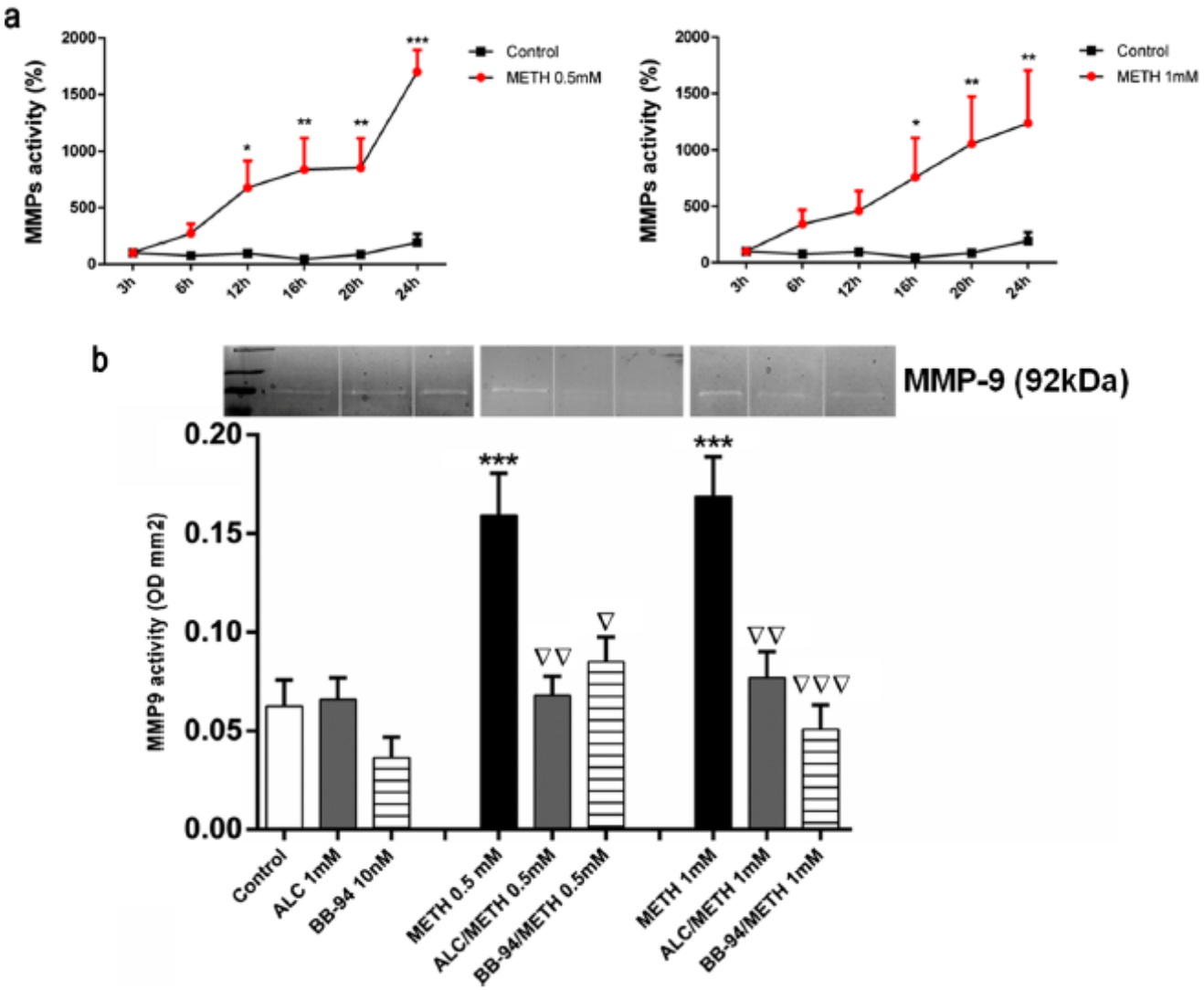

Fig 5 - METH-triggered MMP-9 activity. Confluent bEnd.3 cells monolayers were treated with METH 0.5 and 1 mM and cells; the medium was collected for determination of gelatinases activity. **a Graphic** representation of MMP-9 activity in culture mediums collected at 3, 6, 12, 16, 20, and 24 h after exposure to 0.5 mM METH (*upper left*) and 1 mM METH (*upper right*). **b** Zymography was performed to assess the effect of ALC 1 mM and BB-94 10 nM pretreatment on METH-induced MMP-9 activity at 24 h. Data represent mean ± SEM. Significant differences are marked as $*p < 0.05$; $**p < 0.01$, and $***p < 0.001$ compared to the control; $\nabla p < 0.05$, $\nabla\nabla p < 0.01$, and $\nabla\nabla\nabla p < 0.001$ compared to the respective METH-dose treated cells (as determined by ANOVA followed by the Bonferroni post hoc test)

To test the effect of ALC at the MMP-9 level, we evaluated the release of this gelatinase in

the presence of ALC added before METH exposure. As represented in Fig. 5b, ALC 1 mM was effective in preventing the activation of MMP-9 both for METH 0.5 and 1 mM ($p < 0.01$ for both METH doses vs control). The broad spectrum MMP inhibitor BB-94 was also assayed resulting in the expected inhibition of the METH-triggered MMPs activity ($p < 0.05$ for METH 0.5 mM and $p < 0.001$ for METH 1 mM vs control, Fig. 5b). Importantly, ALC inhibition of MMPs activity was not significantly different from that achieved with BB-94 ($p > 0.9999$).

Next, we tested if the inhibition of MMPs activity would have an impact at the level of TJs. We added the MMP inhibitor BB-94 to the bEnd.3 cell culture before METH treatment and evaluated the distribution of claudin-5 by immunofluorescence analysis. As depicted in Fig. 3a and quantified in Fig. 3b, inhibition of MMPs activity reduced METH-induced translocation of claudin-5 to the cytoplasm, as evidenced by the ratio membrane/cytoplasm for claudin-5 localization ($p < 0.001$ for both METH doses vs control, Fig. 3b). These results confirm that METH-induced translocation of claudin-5 is promoted by METH-triggered activation of MMPs, which was previously shown to have a crucial role in TJ degradation in other pathologic conditions.
Importantly, at this level, the effect of BB-94 was similar to that of ALC ($p = 0.14$).

ALC Prevented ILK Expression Induced by METH

Since ILK increased expression has been reported to increase MMP-9 activation, we investigated the impact of METH on ILK expression in bEnd.3 cells. Our results show that METH treatment induced a significant increase in ILK expression ($p < 0.05$, METH vs control), which was totally prevented when ALC was added to the medium 30 min before METH exposure ($p < 0.05$, METH vs ALC/METH), (Fig. 6a). To our knowledge, the action of METH over ILK expression was never reported. Likewise, the preventive effect of ALC at this level is also a new and exciting feature for this compound.

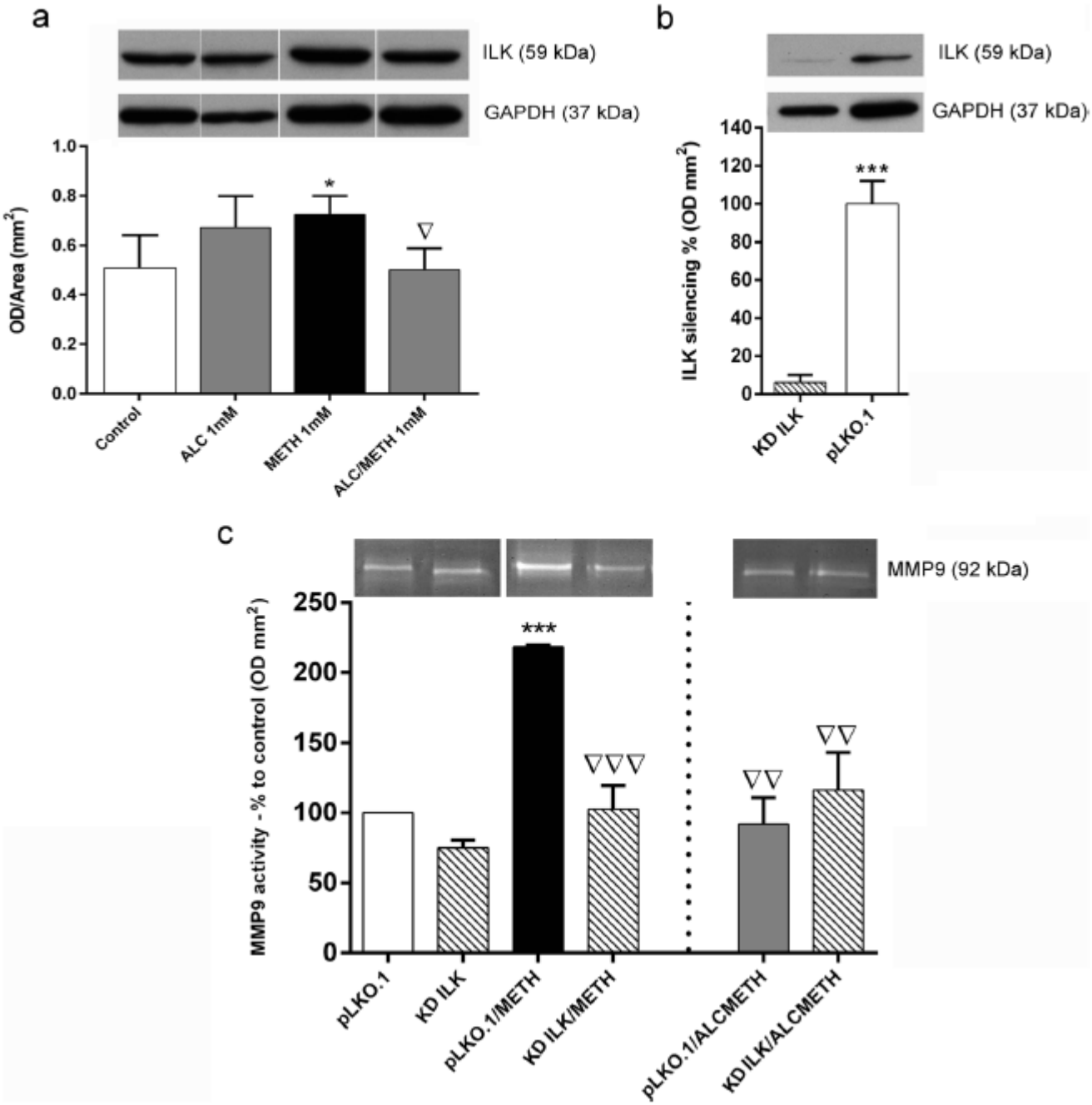

Figura 6 - ALC prevented METH-induced ILK increased expression. Confluent bEnd.3 cells monolayers were treated with METH 1 mM with or without 1 mM ALC. **a** Graphic representation of the total amount of ILK expression 24 h after METH treatment for each condition, significant differences are marked as $*p < 0.05$ compared to the control and $\nabla p < 0.01$ compared to METH treatment. **b** ILK silencing in bEnd.3 cells at 6 days of infection ($**p < 0.01$ and $***p < 0.0001$, compared to the respective non-silenced cells, pLKO.1). **c** Zymography performed in bEnd.3 culture medium after METH and/or ALC treatment in ILK knockdown cells (KD ILK) and control cells (pLKO.1) ($***p < 0.001$ for pLKO.1 vs pLKO.1/METH, $\nabla\nabla\nabla$ $p < 0.001$ for KD ILK vs KD ILK/lviE1H and V'V'p<O.Ol for pLKO.l vs KD ILK/lviE1H and pLKO.liALCME1H). Data represent mean ±SEM. Ali significant differences were determined by ANOVA followed by the Bonfen·oni post hoc test

ILK Silencing Prevented METH-Triggered MMP-9 Activity

Six days after infection, ILK silencing was completed (~90 %) in endothelial cells as shown in Fig. 6b ($p < 0.001$, KD ILK vs pLKO.1). When analyzed by zymography (Fig. 6c), bEnd.3 cells treated with METH showed significantly higher levels of activated MMP-9 than those where ILK was knockdown ($p < 0.001$, pLKO.1/METH vs KD ILK/METH). Therefore, our results show that cells lacking ILK fail to respond to METH by increasing MMP-9 activity. As reported above, ALC was able to prevent the METH-induced activation of MMP-9 ($p < 0.01$ for pLKO.1/METH vs pLKO.1/ALCMETH). In addition, the action of ALC/METH in KD ILK cells is not different from the action of METH in these cells ($p > 0.9999$ for KD ILK/METH vs KD ILK/ALCMETH), showing that ILK may be a target for ALC action.

Discussion

It is commonly accepted that MMP-induced leakiness at the BBB is a critical event for the development of several neurological diseases. In the present study, we provide evidence that ALC is able to prevent the METH-triggered activation of MMP-9 via ILK increased expression, preventing changes in F-actin arrangement and claudin-5 redistribution. To our knowledge, this is the first time that ALC is shown to prevent MMP-associated disruption of TJ and F-actin alignment, which is expected to contribute to maintain the BBB integrity.

In healthy endothelial cells, F-actin is organized along the cell axis into bright oriented bundles, forming aligned filaments that promote traction forces, adhesion, and maintain the stability of cell morphology [44].

METH impact on actin filaments was observed in previous studies that reported either actin depolymerization, altered cell shape, local accumulation of condensed actin, or disruption of the F-actin parallel strands, leading to compromised TJ function [14, 26, 45]. In our study, METH exposure led to a dramatic loss of F-actin integrity concomitant with claudin-5 redistribution and decreased expression. In endothelial cells, these events may lead to loss of adhesion and/or relevant restructuration of the endothelium, thus contributing to increase METH neurotoxicity. Interestingly, although METH-induced internalization of both claudin and occludin through endocytosis was previously seen to be concomitant with TJ fragmentation and gap formation [3, 13, 14], the functional significance of such translocation remains unclear, since it can occur also in the absence of BBB structural changes [15]. As the anchoring protein *ZO-1* and the transmembrane protein occludin are physically linked to the actin filaments, some authors have hypothesized that actin depolymerization could be secondary to the loss of these binding interactions. METH impact on ZO-1, however, is not consensual, and similarly to what we report here, other authors also could not verify any changes in this particular protein [3, 10].

Importantly, our work was the first to report ALC protection over METH-induced changes in TJ function, since a pretreatment with 1 mM ALC was effective in preventing the METH-

induced loss of actin alignment, as well as claudin-5 loss and translocation to the cytoplasm. The action of ALC at the cytoskeleton level is poorly explored, but previous in vitro studies have shown that ALC promotes microtubule stabilization which can render the cells more resistant to insults [30].

Different mechanisms have been proposed for the lack of BBB tightness after METH exposure [3, 4, 10, 11, 13, 15]. Among those, the activation and expression of MMPs, a common mechanism of BBB leakiness, was often referred after METH exposure [4, 6, 9]. Based on previous reports where L-carnitine was seen to decrease glomerular sclerosis and interstitial fibrosis after cisplatin treatment, by reducing MMP-9 activity [46], and ALC administration was shown to ameliorate MMP-related dystrophy [47], we hypothesized that ALC could prevent METH-induced MMPs activity contributing this way to maintain the integrity of the endothelial monolayer. Increased MMP-9 activity after METH exposure was previously reported in brain regions associated to the reward system [6, 9]. MMPs are proteolytic enzymes involved in the remodeling and cleavage of the extracellular matrix known to degrade TJ proteins. Our zymography results show that both METH 0.5 and 1 mM doses triggered the activity of MMP-9, but not of MMP-2.
This is in accordance with former in vivo studies that reported a rapid transient increase in striatal MMP-9 expression and activity after repeated low doses of METH, which was associated with increased degradation of extracellular matrix components and increased BBB permeability [4, 6, 9, 48]. As hypothesized, ALC 1 mM was able to prevent MMP-9 increased activity in cells exposed to METH, which prevented changes on F-actin alignment and reduced claudin-5 redistribution, contributing to maintain the integrity of the endothelial cytoskeleton. These results open new insights into ALC therapeutic use.

Another possible mechanism for METH-induced damage at the BBB level is associated to increased production of ROS by endothelial cells [3, 10, 13, 29]. In a former study, it was proposed that increased oxidative stress in METH-treated endothelial cells could lead to cytoskeleton rearrangement and TJ redistribution through RhoA activation [10]. Modulation of RhoGTPases by METH has been reported showing that RhoA, Rac, or Cdc42 can be modulated by METH, impacting the endothelial barrier [10, 13, 14]. Constitutive activation of RhoGTPases was associated with TJ endocytosis and stress fibers assembly and reorganization [14, 49, 50]. Rho-associated coiled-coil-containing kinases (ROCK) are important cytoskeleton regulators through downstream modulation of actin, myosin, and associated proteins [10, 49–51]. Previous studies have shown the involvement of the Rho/ROCK pathway on actin reorganization and verified that ROCK inhibition was able to block actin disruption [50, 52]. Aiming to evaluate the role of ROCK on METH-induced structural damage, we used the ROCK selective inhibitor fasudil. However, ROCK inhibition did not prevent METH-induced disruption of F-actin organization and led to a highly disturbed structural pattern (Online Resource 1). The influence of RhoGTPases activation and/or inactivation on TJ function is ambiguous. In Madin-Darby canine kidney (MDCK) epithelial cells expressing constitutively active or dominant-negative RhoA, Rac1, or Cdc42, it was shown that activation, as well as inactivation, of each GTPase resulted in increased

paracellular permeability and dramatic reorganization of the F-actin cytoskeleton and TJ proteins [49], evidencing that Rho GTPases in epithelial junctions may regulate the barrier function through distinct mechanisms.

Several possible mechanisms were proposed for METH-triggered MMP-9 activity, involving different signaling cascades depending on stimulus, cell type, and MMP isoform [6, 53]. Mechanisms related with METH-induce glutamate [6] or dopamine [54] release are plausible in vivo, but not feasible in our bEnd.3 model. Increased phosphorylation of p38, JNK1/2, and/or ERK1/2 proteins leading to higher transcription of MMPs was also suggested [4, 47, 53].
Importantly, JNK1/2 and p38 were both reported to suffer increased phosphorylation after METH exposure in vivo [11] and decreased phosphorylation after ALC administration [47]. However, in the present study, we could not observe increased MMP transcription as a consequence of METH exposure (Online Resource 2), suggesting that METH-triggered MMP-9 activity may occur through posttranslational processes.

Cell adhesion to the extracellular matrix is an important process controlling cell shape change, migration, proliferation, survival, and differentiation. Recent studies have revealed that cytoplasmic integrin- linked kinase (ILK) and its interactive proteins play important roles in these processes [55]. ILK is directly binded to the cytoplasmic domains of β1 integrin and connects integrins to the actin cytoskeleton by interacting directly with several proteins such as paxillin and parvin, thus, coordinating actin organization [55, 56]. There is evidence that ILK expression stimulates MMP-9 activation, whereas ILK silencing inhibits invasion in several carcinomas [56, 57]. In normal epithelial cells, the loss of cell–cell adhesion is the hallmark of ILK overexpression, due to the E-cadherin downregulation and nuclear translocation [58]. ILK overexpression and clustering results in the activation of a variety of intracellular signaling processes such as Akt phosphorylation and GSK-3 inhibition, which lead to the activation of the transcription factor AP-1 resulting in the MMP-9 potentiation [55, 57]. In the present work, we show that METH-triggered activation of MMP-9 is mediated by ILK overexpression, which, to our knowledge, was never shown before. Although it was suggested that ILK may upregulate MMP-9 by promoting MMP-9 overexpression, as already mentioned, we failed to observe METH-induced increased transcription of MMP-9 (Online Resource 2). However, other authors have also reported ILK-dependent increased MMP-9 activity in the absence of significant changes in its expression, suggesting that under ILK regulation, various pathways may be involved [58].

BBB impairment after METH exposure may exacerbate drug neurotoxicity and may contribute to the long-term neurodegeneration and cognitive deficits frequently reported. This may occur by increased extravasation of neurotoxic proteins and pro-inflammatory molecules across the barrier, as well as deficits in both transcellular and paracellular transports [7, 15]. We show also that ALC was effective in preventing the increased expression of ILK, thus preventing MMP-9 activation and preserving actin structure and TJ function. The present results support the potential of ALC in preserving the BBB integrity, which was already demonstrated in vivo, since it was shown that alcohol impairment on human brain endothelium is prevented by ALC treatment [28, 29]. Of note, our results highlight ILK as a new target for ALC therapeutic use. The ongoing development of selective inhibitors of both MMP-9 and ILK as potential pharmacologic targets in several

diseases may benefit from ALC investigation particularly in the oncology field, where increased activity of MMPs is long known to be associated with tumor invasion and metastatic potential [59, 60].

Despite the protection obtained at the structural level, ALC was not able to prevent cell death and reduced viability in our bEnd.3 cultures exposed to METH 1 mM. In isolated endothelial cells, loss of viability under METH exposure can be associated with mitochondrial dysfunction caused by deficient antioxidant defense machinery accompanied by substantial lipid peroxidation, protein carbonylation, and increased ROS generation, which leads to disruption of the mitochondrial electrochemical gradient, impaired ATP synthesis, and energy deficits [for review, see 2]. In this scenario, cell death may arise as a consequence of METH-induced release of cytochrome c into the cytosol and resulting activation of caspase-mediated apoptotic pathways. The involvement of nitric oxide (NO) and peroxynitrite in METH-related apoptotic mechanisms has also been reported [61].

Moreover, it has been shown that, through ROS-signaling, METH can regulate the expression of AP-1, NF-κB, and AP-2 families that are crucial in controlling death and survival signals [for review, see 2]. Via JNK activation, ROS-signaling can also induce DNA strand break and base excision [62]. In addition, endothelial cells are important producers of several cytokines and release high amounts of interleukin-1 (IL-1) [63], which is known to be the major endogenous pyrogen [64]. Although we did not collect any data regarding METH-induced hyperthermia, changes in cellular morphology under
METH exposure were shown to tightly correlate with hyperthermia and increased BBB permeability [65]. Noteworthy, we have shown in vivo that ALC neuroprotection over MDMA exposure is not related to the drug-induced thermal response [66]. We have also shown that in vivo ALC prevents DNA damage and carbonyl formation, but not lipid peroxidation [66]. Using a human endothelial cell line, other authors demonstrated that ALC prevents METH-induced loss of cell viability under glucose deprivation [67]. In such conditions, ALC may increase the availability of acyl-CoA to the citric acid cycle counteracting the decreased pyruvate dehydrogenase activity. However, under standard glucose levels, as in the present study, ALC protection against METH-induced cell loss was not shown. As such, we reason that the rate of cell loss observed for METH 1 mM is probably due to increased ROS/RNS-signaling at the mitochondrial level, through the activation of pathways that cannot be regulated by ALC.

Conclusion

In summary, we showed that in endothelial cells, exposure to METH led to disruption of actin filaments concomitant with claudin-5 translocation to the cytoplasm. These events seem to be mediated by MMP-9 activation in association with ILK overexpression and may lead to TJ dysfunction and BBB increased permeability. Our work was the first to assess the role of ALC as a neuroprotective agent over METH-induced damage via MMP-9 activity.

Pretreatment with ALC prevented METH-induced activation of MMP-9, preserving claudin-5 location and the structural arrangement of the actin filaments (Fig. 7). Our results highlight ILK as a nouvelle target for ALC therapeutic use, adding to the list of ALC benefits in several neurologic conditions. Of note, this may be of particular interest in the oncology field due to the close relation between MMP-9 activity and metastatic events.

Fig. 7

Schematic representation of the ALC protective role over the molecular events triggered by METH in endothelial cells. Exposure to METH in bEnd.3 leads to disruption of the actin filaments arrangement and claudin-5 translocation to the cytoplasm (and decreased expression). We show that these events are mediated by MMP-9 activation in association with ILK overexpression and may lead to tight junction dysfunction and increased BBB permeability. Pretreatment with ALC prevented METH-induced activation of MMP-9 and preserved the arrangement of actin filaments and claudin-5 distribution. Our results highlight ILK as a nouvelle target for the ALC therapeutic use

Acknowledgments

This research project was funded by Programa Operacional Factores de Competitividade (COMPETE) and by National funds through FCT—Fundação para a Ciencia e Tecnologia, reference FCOMP-01-0124-FEDER-011320 (FCT PTDC/SAU-OSM/100630/2008). Joana Bravo received a research grant under this project. Teresa Summavielle was supported by Programa Ciência—Programa Operacional Potencial Humano (POPH)-Promotion of Scientific Employment, ESF and MCTES and program Investigador FCT, POPH and Fundo Social Europeu. We thank Glial Cell Biology Group as a whole and specially Dr Joana Paes Faria and Dr João Relvas for providing the lentivirus for shRNA-mediated silencing of ILK. We thank Dr Fátima Pina (INEB, University of Porto) for statistic advice in the analyses of the actin data. We thank Dr Maria José Oliveira (INEB, University of Porto) for her kind support regarding the zymography methodology. We also thank Dr

Paula Sampaio and Paula Magalhães (IBMC Technical Services) for assistance with image analyses and cell culture facilities.

References

1. Gold MS, Kobeissy FH, Wang KK, Merlo LJ, Bruijnzeel AW, Krasnova IN, Cadet JL (2009) Methamphetamine- and trauma-induced brain injuries: comparative cellular and molecular neurobiological substrates. Biol Psychiatry 66(2):118–127. doi: 10.1016/j.biopsych.2009.02.021

2. Krasnova IN, Cadet JL (2009) Methamphetamine toxicity and messengers of death. Brain Res Rev 60(2):379–407. doi:10.1016/j.brainresrev.2009.03.002

3. Ramirez SH, Potula R, Fan S, Eidem T, Papugani A, Reichenbach N, Dykstra H, Weksler BB, Romero IA, Couraud PO, Persidsky Y (2009) Methamphetamine disrupts blood-brain barrier function by induction of oxidative stress in brain endothelial cells. J Cereb Blood Flow Metab 29(12):1933–1945. doi: 10.1038/jcbfm.2009.112

4. Urrutia A, Rubio-Araiz A, Gutierrez-Lopez MD, ElAli A, Hermann DM, O'Shea E, Colado MI (2013) A study on the effect of JNK inhibitor, SP600125, on the disruption of blood-brain barrier induced by methamphetamine. Neurobiol Dis 50:49–58. doi: 10.1016/j.nbd.2012.10.006

5. Bowyer JF, Thomas M, Schmued LC, Ali SF (2008) Brain region- specific neurodegenerative profiles showing the relative importance of amphetamine dose, hyperthermia, seizures, and the blood-brain barrier. Ann N Y Acad Sci 1139:127–139. doi: 10.1196/annals.1432.005

6. Conant K, Lonskaya I, Szklarczyk A, Krall C, Steiner J, Maguire-Zeiss K, Lim ST (2011) Methamphetamine-associated cleavage of the synaptic adhesion molecule intercellular adhesion molecule-5. J Neurochem 118(4):521–532. doi: 10.1111/j.1471-4159.2010.07153.x

7. Northrop NA, Yamamoto BK (2012) Persistent neuroinflammatory effects of serial exposure to stress and methamphetamine on the blood-brain barrier. J Neuroimmune Pharmacol 7(4):951–968. doi: 10.1007/s11481-012-9391-y

8. Goncalves J, Baptista S, Martins T, Milhazes N, Borges F, Ribeiro CF, Malva JO, Silva AP (2010) Methamphetamine-induced neuroinflammation and neuronal dysfunction in the mice hippocampus: preventive effect of indomethacin. Eur J Neurosci 31(2):315–326. doi: 10.1111/j.1460-9568.2009.07059.x

9. Martins T, Baptista S, Goncalves J, Leal E, Milhazes N, Borges F, Ribeiro CF, Quintela O, Lendoiro E, Lopez-Rivadulla M, Ambrosio AF, Silva AP (2011) Methamphetamine transiently increases the blood-brain barrier permeability in the hippocampus: role of tight junction proteins and matrix metalloproteinase-9. Brain Res 1411:28–40. doi: 10.1016/j.brainres.2011.07.013

10. Mahajan SD, Aalinkeel R, Sykes DE, Reynolds JL, Bindukumar B, Adal A, Qi M, Toh J, Xu G, Prasad PN, Schwartz SA (2008) Methamphetamine alters blood brain barrier permeability via the modulation of tight junction expression: implication for HIV-1 neuropathogenesis in the context of drug abuse. Brain Res 1203:133–148. doi: 10.1016/j.brainres.2008.01.093

11. ElAli A, Urrutia A, Rubio-Araiz A, Hernandez-Jimenez M, Colado MI, Doeppner TR, Hermann DM (2012) Apolipoprotein-E controls adenosine triphosphate-binding cassette transportes ABCB1 and ABCC1 on cerebral microvessels after methamphetamine intoxication. Stroke 43(6):1647–1653. doi: 10.1161/STROKEAHA.111.648923

12. Haorah J, Knipe B, Leibhart J, Ghorpade A, Persidsky Y (2005) Alcohol-induced oxidative stress in brain endothelial cells causes blood-brain barrier dysfunction. J Leukoc Biol 78(6):1223–1232. doi: 10.1189/jlb.0605340

13. Toborek M, Seelbach MJ, Rashid CS, András IE, Chen L, Park M, Esser KA (2013) Voluntary exercise protects against methamphetamine-induced oxidative stress in brain microvasculature and disruption of the blood-brain-barrier. Mol Neurodegener 8(1):22. doi: 10.1186/1750-1326-8-22

14. Park M, Kim HJ, Lim B, Wylegala A, Toborek M (2013) Methamphetamine-induced occludin endocytosis is mediated by the Arp2/3 complex-regulated actin rearrangement. J Biol Chem 288(46):33324–33334. doi: 10.1074/jbc.M113.483487

15. Martins T, Burgoyne T, Kenny B-A, Hudson N, Futter CE, Ambrósio AF, Silva AP, Greenwood J, Turowski P(2013) Methamphetamine-induced nitric oxide promotes vesicular transport in blood-brain barrier endothelial cells. Neuropharmacol (65):74-82. doi: 10.1016/j.neuropharm.2012.08.021

16. Balda MS, Whitney JA, Flores C, González S, Cereijido M, Matter K (1996) Functional dissociation of paracellular permeability and transepithelial electrical resistance and disruption of the apical-basolateral intermembrane diffusion barrier by expression of a mutant tight junction membrane protein. J Cell Biol 134(4):1031–1049

17. Chen F, Hori T, Ohashi N, Baine AM, Eckman CB, Nguyen JH (2011) Occludin is regulated by epidermal growth factor receptor activation in brain endothelial cells and brains of mice with acute liver failure. Hepatology 53(4):1294–1305. doi: 10.1002/hep.24161

18. Yamamoto M, Ramirez SH, Sato S, Kiyota T, Cerny RL, Kaibuchi K, Persidsky Y, Ikezu T (2008) Phosphorylation of claudin-5 and occludin by rho kinase in brain endothelial cells. Am J Pathol 172(2):521–533. doi: 10.2353/ajpath.2008.070076

19. Muresan Z, Paul DL, Goodenough DA (2000) Occludin 1B, a Variant of the Tight Junction Protein Occludin. Mol Biol Cell 11:627-634

20. Reynolds JL, Mahajan SD, Aalinkeel R, Nair B, Sykes DE, Schwartz SA (2011) Methamphetamine and HIV-1 gp120 effects on lipopolysaccharide stimulated matrix metalloproteinase-9 production by human monocyte-derived macrophages. Immunol Invest

40(5):481–497. doi: 10.3109/08820139.2011.559499

21. Liebner S, Kniesel U, Kalbacher H, Wolburg H (2000) Correlation of tight junction morphology with the expression of tight junction proteins in blood-brain barrier endothelial cells. Eur J Cell Biol 79(10):707–717. doi: 10.1078/0171-9335-00101

22. Kashiwamura Y, Sano Y, Abe M, Shimizu F, Haruki H, Maeda T, Kawai M, Kanda T (2011) Hydrocortisone enhances the function of the blood-nerve barrier through the up-regulation of claudin-5. Neurochem Res 36(5):849–855. doi: 10.1007/s11064-011-0413-6

23. Masahiko I, Kazumasa M, Schoichiro T (1999) Characterization of ZO-2 as a MAGUK family member associated with tight as well as adherens junctions with a binding affinity to occludin and a catenin. J Biol Chem 274(26):5981–5986

24. Singh AB, Harris RC (2004) Epidermal growth factor receptor activation differentially regulates claudin expression and enhances transepithelial resistance in Madin-Darby canine kidney cells. J Biol Chem 279(5):3543–3552. doi: 10.1074/jbc.M308682200

25. Forster C, Burek M, Romero IA, Weksler B, Couraud PO, Drenckhahn D (2008) Differential effects of hydrocortisone and TNFalpha on tight junction proteins in an in vitro model of the human blood-brain barrier. J Physiol 586(7):1937–1949. doi: 10.1113/jphysiol.2007.146852

26. Young EJ, Aceti M, Griggs EM, Fuchs RA, Zigmond Z, Rumbaugh G, Miller CA (2014) Selective, retrieval-independent disruption of methamphetamine-associated memory by actin depolymerization. Biol Psychiatry 75(2):96–104. doi: 10.1016/j.biopsych.2013.07.036

27. Mizoguchi H, Yamada K, Nabeshima T (2011) Matrix metalloproteinases contribute to neuronal dysfunction in animal models of drug dependence, Alzheimer's disease, and epilepsy. Biochem Res Int 2011:681385. doi: 10.1155/2011/681385

28. Abdul Muneer PM, Alikunju S, Szlachetka AM, Haorah J (2011) Inhibitory effects of alcohol on glucose transport across the blood-brain barrier leads to neurodegeneration: preventive role of acetyl-L: -carnitine. Psychopharmacology (Berl) 214(3):707–718. doi: 10.1007/s00213-010-2076-4

29. Haorah J, Floreani NA, Knipe B, Persidsky Y (2011) Stabilization of superoxide dismutase by acetyl-l-carnitine in human brain endothelium during alcohol exposure: novel protective approach. Free Radic Biol Med 51(8):1601–1609. doi:10.1016/j.freeradbiomed.2011.06.020

30. Pettegrew J, Levine J, McClure R (2000) Acetyl-L-carnitine physical-chemical,

metabolica, and therapeutic properties: relevance for its mode of action in Alzheimer's disease and geriatric depression. Mol Psych 5:616–632

31. Jones LL, McDonald DA, Borum PR (2010) Acylcarnitines: role in brain. Prog Lipid Res 49(1):61–75. doi: 10.1016/j.plipres.2009.08.004

32. Goo MJ, Choi SM, Kim SH, Ahn BO (2012) Protective effects of acetyl-L-carnitine on neurodegenarative changes in chronic cerebral ischemia models and learning-memory impairment in aged rats. Arch Pharm Res 35(1):145–154. doi:10.1007/s12272-012-0116-9

33. Lee NY, Choi HO, Kang YS (2012) the acetylcholinesterase inhibitors competitively inhibited an acetyl L-carnitine transport through the blood-brain barrier. Neurochem Res 37(7):1499–1507. doi: 10.1007/s11064-012-0723-3

34. Yasuto K, Ikumi T, Aki O, Yoshimichi S, Toru K, Jun-ichi N, Hiroko N, Noriyoshi H, Masahide A, Akira T (2001) Functional relevance of carnitine transporter OCTN2 to brain distribution of L-carnitine and acetyl-L-carnitine across the blood-brain barrier. J Neurochem 79:959–969

35. Kusuhara H, Sugiyama Y (2005) Active efflux across the blood-brain barrier: role of the solute carrier family. ASENT 2:73–85

36. Rump TJ, Abdul Muneer PM, Szlachetka AM, Lamb A, Haorei C, Alikunju S, Xiong H, Keblesh J, Liu J, Zimmerman MC, Jones J, Donohue TM Jr, Persidsky Y, Haorah J (2010) Acetyl-L-carnitine protects neuronal function from alcohol-induced oxidative damage in the brain. Free Radic Biol Med 49(10):1494–1504. doi: 10.1016/j.freeradbiomed.2010.08.011

37. Brown RC, Morris AP, O'Neil RG (2007) Tight junction protein expression and barrier properties of immortalized mouse brain microvessel endothelial cells. Brain Res 1130(1):17–30. doi:10.1016/j.brainres.2006.10.083

38. Omidi Y, Campbell L, Barar J, Connell D, Akhtar S, Gumbleton M (2003) Evaluation of the immortalised mouse brain capillary endothelial cell line, b.End3, as an in vitro blood–brain barrier model for drug uptake and transport studies. Brain Res 990(1–2):95–112. doi: 10.1016/s0006-8993(03)03443-7

39. Jin CH, Moo TT, Youn CS, Sun YJ, Joo-Il K, Sook HE, Onyou H (2002) Methamphetamine-induced apoptosis in a CNS-derived catecholaminergic cell line. Mol Cells 13(2):221–227

40. Huang H, Liu N, Guo H, Liao S, Li X, Yang C, Liu S, Song W, Liu C, Guan L, Li B, Xu L, Zhang C, Wang X, Dou QP, Liu J (2012) L-carnitine is an endogenous HDAC inhibitor selectively inhibiting cancer cell growth in vivo and in vitro. PLoS One 7(11):e49062. doi:10.1371/journal.pone.0049062

41. Wojtowicz-Praga SM, Dickson RB, Hawkins MJ (1997) Matrix metalloproteinase inhibitors. Investig New Drugs 15:61–75

42. Doug L (2000) Comparison of the LDH and MTT assays for quantifying cell death: validity for neuronal apoptosis? J Neurosc Meth 96:147–152

43. Nekouzadeh A, Genin GM (2011) Quantification of fibre polymerization through Fourier space image analysis. Proc Math Phys Eng Sci 467(2132):2310–2329. doi: 10.1098/rspa.2010.0623

44. Shamloo A (2014) Cell-cell interactions mediate cytoskeleton organization and collective endothelial cell chemotaxis. Cytoskeleton (Hoboken). doi: 10.1002/cm.21185

45. Shen L, Turner JR (2005) Actin depolymerization disrupts tight junctions via caveolae-mediated endocytosis. Mol Biol Cell 16(9):3919–3936. doi: 10.1091/mbc.E04-12-1089

46. Martinez G, Costantino G, Clementi A, Puglia M, Clementi S, Cantarella G, De Meo L, Matera M (2009) Cisplatin-induced kidney injury in the rat: L-carnitine modulates the relationship between MMP-9 and TIMP-3. Exp Toxicol Pathol 61(3):183–188. doi: 10.1016/j.etp.2008.07.004

47. Hnia K, Hugon G, Rivier F, Masmoudi A, Mercier J, Mornet D (2007) Modulation of p38 mitogen-activated protein kinase cascade and metalloproteinase activity in diaphragm muscle in response to free radical scavenger administration in dystrophin-deficient Mdx mice. Am J Pathol 170(2):633–643. doi: 10.2353/ajpath.2007.060344

48. Abdul Muneer PM, Alikunju S, Szlachetka AM, Haorah J (2012) The mechanisms of cerebral vascular dysfunction and neuroinflammation by MMP-mediated degradation of VEGFR-2 in alcohol ingestion. Arterioscler Thromb Vasc Biol 32(5):1167–1177. doi:10.1161/ATVBAHA.112.247668

49. Bruewer M, Hopkins AM, Hobert ME, Nusrat A, Madara JL (2004) RhoA, Rac 1, and Cdc42 exert distinct effects on epithelial barrier via selective strictural and biochemical modulation on junctional proteins and F-actin. Am J Physiol Cell Physiol 287:C327-C335

50. Breyer J, Samarin J, Rehm M, Lautscham L, Fabry B, Goppelt- Struebe M (2012)

Inhibition of Rho kinases increases directional motility of microvascular endothelial cells. Biochem Pharmacol 83(5):616–626. doi: 10.1016/j.bcp.2011.12.012

51. Tonges L, Koch JC, Bahr M, Lingor P (2011) ROCKing regeneration: Rho kinase inhibition as molecular target for neurorestoration. Front Mol Neurosci 4:39. doi: 10.3389/fnmol.2011.00039

52. Weiner JA, Fukushima N, Contos JJ, Scherer SS, Chun J (2001) Regulation of Schwann cell morphology and adhesion by receptor-mediated lysophosphatidic acid signaling. J Neurosc 21(18):7069–7078

53. Elke G, Katrin H, Yvette N, Hermann H (2000) Sustained ERK phosphorylation is necessary but not sufficient for MMP-9 regulation in endothelial cells: involvement of Ras-dependent and -independent pathways. J Cell Sci 113:4319–4330

54. Betzen C, White R, Zehendner CM, Pietrowski E, Bender B, Luhmann HJ, Kuhlmann CR (2009) Oxidative stress upregulates the NMDA receptor on cerebrovascular endothelium. Free Radic Biol Med 47(8):1212–1220. doi:10.1016/j.freeradbiomed.2009.07.034

55. Wu C, Dedhar S (2001) Integrin-linked kinase (ILK) and its interactors: a new paradigm for the coupling of extracellular matrix to actin cytoskeleton and signaling complexes. J Cell Biol 155(4):505–510. doi: 10.1083/jcb.200108077

56. Rosano L, Spinella F, Di Castro V, Dedhar S, Nicotra MR, Natali PG, Bagnato A (2006) Integrin-linked kinase functions as a downstream mediator of endothelin-1 to promote invasive behavior in ovarian carcinoma. Mol Cancer Ther 5(4):833–842. doi: 10.1158/1535-7163.MCT-05-0523

57. Troussard AA, Costello P, Yoganathan EN, Kumagai S, Roskelley CD, Dedhar S (2000) The integrin linked kinase (ILK) induces an invasive phenotype via AP-1 transcription factor- dependent upregulation of matrix metalloproteinase 9 (MMP-9). Oncogene 19:5444–5452

58. Matsui Y, Assi K, Ogawa O, Raven PA, Dedhar S, Gleave ME, Salh B, So AI (2012) The importance of integrin-linked kinase in the regulation of bladder cancer invasion. Int J Cancer 130(3):521–531. doi: 10.1002/ijc.26008

59. Johnsen M, Lund RL, Romer J, Almholt K, Danø K (1998) Cancer invasion and tissue remodeling: common themes in proteolytic matrix degradation. Curr Opin Cell Biol 10:667–671

60. Murphy G, Ward R, Hembry RM, Reynolds JJ, Kuhn K, Tryggvason K (1989) Characterization of gelatinase from pig polymorphonuclear leucocytes. Biochem J 258:463–472

61. Sheng P, Cerruti C, Ali S, Cadet JL (1996) Nitric oxide is a mediator of methamphetamine (METH)-induced neurotoxicity. In vitro evidence from primary cultures of mesencephalic cells. Ann N Y Acad Sci 801:174–186

62. Barzilai A (2007) The contribution of the DNA damage response to neuronal viability. Antioxid Redox Signal 9(2):211–218. doi: 10.1089/ars.2007.9.ft-6

63. Mantovani A, Bussolino F, Dejana E (1992) Cytokine regulation of endothelial cell function. FASEB J 6(8):2591–2599

64. Leon LR (2002) Invited review: cytokine regulation of fever: studies using gene knockout mice. J Appl Physiol (1985) 92(6):2648–2655. doi: 10.1152/japplphysiol.01005.2001

65. Sharma HS, Kiyatkin EA (2009) Rapid morphological brain abnormalities during acute methamphetamine intoxication in the rat: an experimental study using light and electron microscopy. J Chem Neuroanat 37(1):18–32. doi: 10.1016/j.jchemneu.2008.08.002

66. Alves E, Binienda Z, Carvalho F, Alves CJ, Fernandes E, de Lourdes BM, Tavares MA, Summavielle T (2009) Acetyl-L-carnitine provides effective in vivo neuroprotection over 3, 4-methylenedioximethamphetamine-induced mitochondrial neurotoxicity in the adolescent rat brain. Neuroscience 158(2):514–523. doi: 10.1016/j.neuroscience.2008.10.041

67. Abdul Muneer PM, Alikunju S, Szlachetka AM, Murrin LC, Haorah J (2011) Impairment of brain endothelial glucose transporter by methamphetamine causes blood-brain barrier dysfunction. Mol Neurodegener 6:23. doi: 10.1186/1750-1326-6-23